Available online at www.sciencedirect.com
ScienceDirect
Ceramics International 35 (2009) 1481–1486
CERAMICS INTERNATIONAL
www.elsevier.com/locate/ceramint

Impedance analysis of Sr-substituted $CePO_4$ with mixed protonic and p-type electronic conduction

Esmeralda Gómez del Moral [a], Duncan P. Fagg [a], Eva Chinarro [a], João C.C. Abrantes [b], José Ramón Jurado [a], Glenn C. Mather [a,*]

[a] *Instituto de Cerámica y Vidrio, CSIC, Cantoblanco, 28049 Madrid, Spain*
[b] *UIDM, ESTG, Polytechnic Institute of Viana do Castelo, 4900 Viana do Castelo, Portugal*

Received 3 January 2008; received in revised form 16 July 2008; accepted 4 August 2008
Available online 31 August 2008

Abstract

Members of the solid-solution series $Ce_{1-x}Sr_xPO_{4-\delta}$ ($x = 0, 0.01, 0.02$) with mixed protonic and electronic transport have been synthesized by a nitrate-decomposition method followed by sintering at 1450 °C. Impedance spectroscopy is employed to estimate the bulk electrical conductivity in wet (~0.03 atm) and dry atmospheres of O_2 and 10%H_2:90%N_2. Conductivity increases with dopant concentration (x), oxygen partial pressure (pO_2) and water vapour partial pressure (pH_2O) reaching $\sim 3.5 \times 10^{-3}$ S cm^{-1} at 600 °C for $x = 0.02$ in wet O_2. Activation energies (E_a) for the bulk conductivity of $Ce_{0.98}Sr_{0.02}PO_{4-\delta}$ below 650 °C are 0.44 and 0.78 eV for wet oxidising and wet reducing conditions, respectively. A moderate but positive pO_2^{+n} power-law dependence ($n < 1/10$) of conductivity is exhibited in the pO_2 range $10^{-2.5}$ to 10^{-1} atm, consistent with mixed ionic and p-type electronic transport. Thermogravimetric analysis indicates that the Sr-doped materials are stable in a CO_2 atmosphere in the temperature range 25–1200 °C.

Keywords: Cerium phosphate; Mixed conductor; Hydrogen-separation membrane; Proton conduction; Impedance spectroscopy

1. Introduction

Hydrogen is considered as one of the most likely energy sources which will lower fossil-fuel dependence, with beneficial effects for climate change, air pollution and energy security. Hydrogen separation and purification currently involves pressure-swing adsorption and cryogenic distillation, with membrane-based technologies in development as a more economic alternative [1]. Types of membrane include polymers, Pd-based systems and microporous inorganic materials. Dense ceramic hydrogen-permeable membranes provide an analogue of the widely investigated oxygen-permeable membranes which may be used for oxygen production, purification and partial oxidation of hydrocarbons [2]. Operation of H_2-permeable devices occurs non-galvanically under a gradient in hydrogen chemical potential, thus materials with mixed electronic and protonic conductivity and good stability in reducing conditions are required.

The search for a suitable ceramic material has focused on perovskites with mixed protonic and n-type electronic conductivity, such as $BaCe_{0.8}Y_{0.2}O_{3-\delta}$ [3]. However, the basicity of these systems leads to poor chemical stability, particularly in acidic gases such as CO_2 [4], and the electronic component of the conductivity is not high enough to maintain a sufficient hydrogen flux. Attempts to circumvent this latter problem have included adding Ni metal to the perovskite in a dense cermet structure with enhanced electronic conductivity [5].

As highlighted recently by Matsumoto et al. [6], the coexistence of electrons and protons is unfavourable in oxide proton conductors. The defect equilibria

$$H_2 + 2h^\bullet = 2H^\bullet \quad (1)$$

and

$$h^\bullet + e' = 0 \quad (2)$$

require that the product of $[H^\bullet][e']$ is constant at a given pO_2. The key to developing dense ceramic membranes with high hydrogen permeability may thus lie in finding a material with appreciable protonic and p-type electronic conductivity.

* Corresponding author. Tel.: +34 917355840; fax: +34 917355843.
E-mail address: mather@icv.csic.es (G.C. Mather).

0272-8842/$34.00
doi:10.1016/j.ceramint.2008.08.004

Accordingly, the electronic component of the hydrogen permeability of $BaCe_{0.9-x}Y_{0.1}Ru_xO_{3-\delta}$ is attributable to an electron hole generated in the O 2p band rather than n-type conductivity [6]. As pointed out by Norby [2], cations with a relatively stable, but oxidisable valence state should thus be employed in the membrane. For example, the stability of the +3 valence state of Cr in reducing conditions is exploited in the p-type conducting SOFC interconnect material, Sr-doped $LaCrO_3$.

Another phase recently reported to exhibit mixed electron hole and proton conduction in both oxidising and reducing conditions is 1 mol% Sr-doped $CePO_4$ [7]. The $CePO_4$ system appears to be promising as a membrane material due to its high stability and low cost. A further potential use for acceptor-substituted $CePO_4$ is as a cathode for an SOFC with a proton-conducting $LaPO_4$-based electrolyte [8]. The La-containing system has been the focus of several studies, whereas the work of Kitamura et al. [7] is the first to report acceptor-substituted $CePO_4$. In this paper, we employ an alternative synthesis route for obtaining Sr-doped $CePO_4$ based on nitrate decomposition and combustion, examine the extent of Sr solubility in the $CePO_4$ host, conduct electrical conductivity studies and determine the stability of the Sr-doped material in CO_2. Electrochemical characterisation is performed by impedance spectroscopy as a function of temperature in wet and dry H_2 and O_2 to delineate bulk contributions to conductivity and their atmospheric and temperature dependencies. Impedance data collected as a function of pO_2 are interpreted in terms of the defect chemistry of the orthophosphate system.

2. Experimental procedure

Compositions of nominal formula $Ce_{1-x}Sr_xPO_{4-\delta}$ ($x = 0$, 0.01, 0.02, 0.05, 0.1) were prepared from appropriate quantities of $Ce(NO_3)_3{\cdot}6H_2O$, $Sr(NO_3)_2$ and $(NH_4)_2HPO_4$. The components were mixed on a hot plate at 150 °C with the addition of urea whose exothermic combustion was used to assist reaction [9]. The temperature was raised to ~300 °C to promote reaction, which occurred in a time of approximately 4 min. The product was milled in an agate mortar then heated at 800 °C for 4 h (heating and cooling rates of 5 °C min^{-1}) in order to remove organic product and achieve further homogenization prior to sintering. Pellets of 15 mm diameter were then prepared from this powder with a uniaxial press. Final firing of the pellets took place in a temperature range of 1200–1500 °C.

Samples were examined for completeness of reaction and phase purity by powder X-ray diffraction (XRD) with a Siemens D5000 instrument (Cu Kα radiation, routine 2θ range of 10–80°). Density was measured by the Archimedes method on displacement of water; relative density values were then calculated as a percentage of the theoretical X-ray density. Microstructure was analysed by scanning electron microscopy (SEM) with a Zeiss DSM400 instrument.

Pellets for conductivity measurements were coated with Pt paste (SPi supplies) and fired at 800 °C for ~1 h to remove the organic content, harden the Pt paste and attach the Pt to the pellet faces. Impedance spectroscopy was performed with an Agilent 4294A instrument, computer controlled with the software Sweep [10]; impedance spectra were routinely measured over the frequency range $40 \leq f \leq 10^6$ Hz, although measurements up to 10^8 Hz were also periodically conducted. Data were collected in the temperature range 300–800 °C in a single-atmosphere cell equipped with a YSZ oxygen sensor in wet and dry O_2, and mixtures of wet and dry $10\%H_2$:$90\%N_2$; dry gases were fed directly to the chamber at a flow rate of 50 ml/min; for wet atmospheres, the gases were firstly bubbled through water at room temperature to provide a water content of ~0.03 atm [11]. Measurements were taken on cooling in steps of 50 °C. On changing atmosphere, data were collected once steady state had been reached (over a period of at least 12 h). Analysis of spectra was performed with the ISA [12] and EQUIVCRT [13] programs to resolve the impedance response into bulk, grain-boundary and electrode contributions.

Measurements were also taken as a function of pO_2 by firstly equilibrating the furnace in a reducing atmosphere ($10\%H_2$:$90\%N_2$) then switching off the gas flow and allowing the atmosphere inside the chamber to slowly equilibrate with the outside air, in a manner similar to that reported previously [14]; equilibration with the atmosphere took place in a period of >14 h, and data were collected at intervals of at least 30 min.

Thermogravimetric analysis (TGA) was performed in high-purity, dried CO_2 with a flow rate of 2 l/h up to 1200 °C (heating rate 5 °C min^{-1}) in a SetSys 16/18 instrument. A comparison of stability in CO_2 was made with the proton-conducting $SrCe_{0.9}Yb_{0.1}O_{3-\delta}$ system, which was synthesized by solid-state reaction in a manner similar to that described previously [15].

3. Results

3.1. Phase formation

The powder XRD patterns of reaction products at 300 °C indicated that $CePO_4$-based material forms with an X-ray pattern consistent with the monoclinic cell of the monazite structure ($CePO_4$, PDF no. 32-0199). Additional peaks indicating incomplete reaction and/or second phases were also observed at this stage for all x (Fig. 1(a)). The width of the

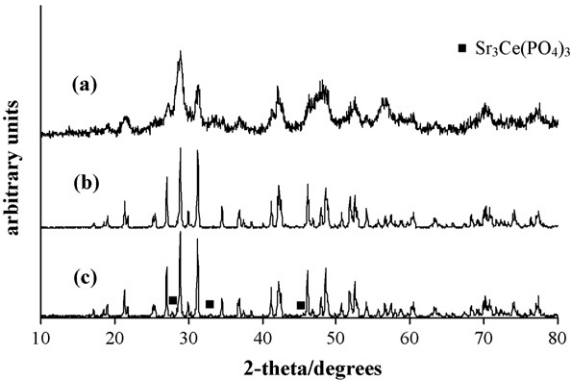

Fig. 1. XRD patterns of (a) $Ce_{0.98}Sr_{0.02}PO_{4-\delta}$ after nitrate decomposition and combustion, (b) $Ce_{0.98}Sr_{0.02}PO_{4-\delta}$ on sintering at 1450 °C, and (c) $Ce_{0.95}Sr_{0.05}PO_{4-\delta}$ on sintering at 1450 °C. Unmarked reflections indicate $CePO_4$-type phase.

X-ray reflections suggests that the crystallite size is in the nanometric range.

On sintering $CePO_4$ at 1500 °C for 6 h, phase-pure product is obtained. The XRD patterns of compositions $x = 0.01$ and 0.02 (Fig. 1 (b)) with final sintering temperature of 1450 °C were indexed on a similar cell to the parent phase. A second phase, $Sr_3Ce(PO_4)_3$, was identified in the patterns of compositions $x = 0.01$ and 0.02 fired at 1500 °C, and for $x = 0.05$ (Fig. 1 (c)) and $x = 0.10$ fired in the range 1200–1500 °C; these materials were not subjected to further study. The intensity of the strongest $Sr_3Ce(PO_4)_3$ reflection for composition $x = 0.05$ was >6% of the most intense peak of the major phase, suggesting that the solid-solution limit is much closer to 2 mol% Sr. The Sr-doped materials were green in colour in contrast to white $CePO_4$.

Pellets densities were determined as ~86–89% of the theoretical X-ray density for samples $x = 0.0$, 0.01 and 0.02. Scanning electron micrographs revealed the presence of open porosity and an average grain size in the micron range, as shown in Fig. 2. Whereas a greater density would be required for a membrane-separation device, the open porosity favours faster equilibration with the gas phase, of relevance when measuring the conductivity as a function of pO_2.

3.2. Impedance spectroscopy

The impedance spectra of $CePO_4$ in oxidising conditions were dominated by a single, slightly-depressed arc, Fig. 3(a). As is common for the analysis of "non-ideal" behaviour [16,17], the response was modelled with an RQ element of resistance R in which the ideal capacitance is replaced by a pseudo-capacitance Q. The true capacitance is related to Q through the angular frequency (ω_o) by the additional parameter n

$$\omega_o = \frac{1}{RC} = (RQ)^{-1/n} \quad (3)$$

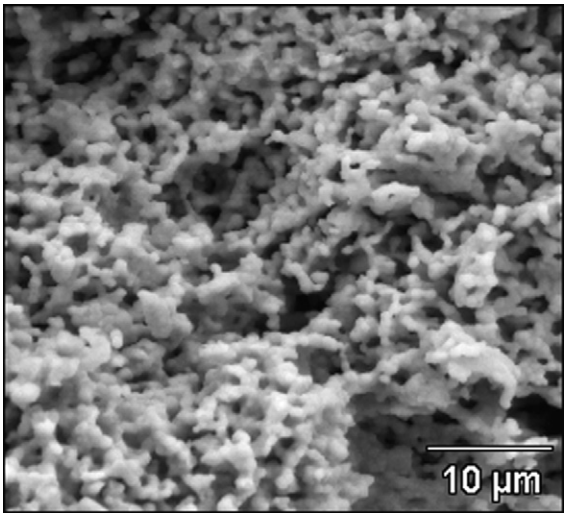

Fig. 2. Scanning electron micrograph of a fracture surface of $Ce_{0.99}Sr_{0.01}PO_{4-\delta}$.

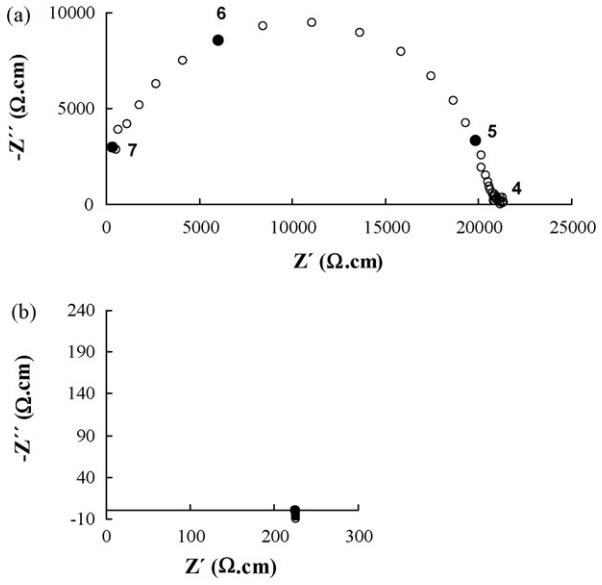

Fig. 3. (a) Impedance spectra in dry O_2 at 650 °C of (a) $CePO_4$ and (b) $Ce_{0.98}Sr_{0.02}PO_{4-\delta}$. Numbers refer to $\log_{10}$ of the frequency.

The capacitance was estimated according to [17]

$$C = Q^{1/n}R^{1-n/n} \quad (4)$$

giving values of ~22 pF, typical of a bulk response. The much lower resistance of the Sr-doped compositions was taken as the intercept on the real, Z′, axis of the impedance spectra (Fig. 3(b)).

The temperature dependencies of conductivity for the $Ce_{1-x}Sr_xPO_{4-\delta}$ series in oxidising conditions, shown in Fig. 4, exhibit Arrhenius behaviour. Corresponding activation energies of conductivity of the title phases in various conditions of temperature and atmosphere are listed in

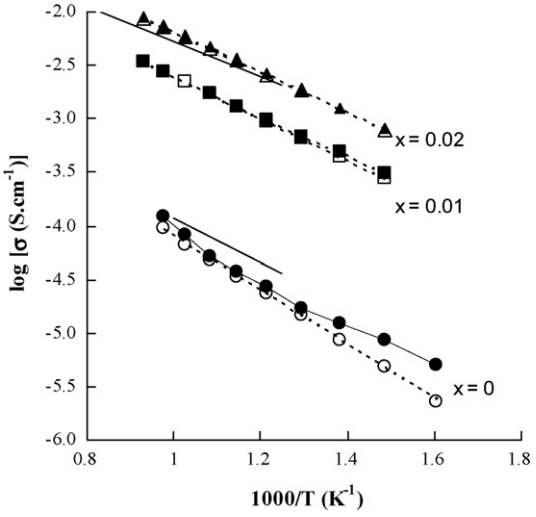

Fig. 4. Temperature dependence of conductivity of the $Ce_{1-x}Sr_xPO_{4-\delta}$ series in wet (closed symbols) and dry (open symbols) O_2. Total and bulk conductivities are plotted for Sr-doped and doped compositions, respectively. Solid lines represent data taken from ref. [7] for $CePO_4$ and $Ce_{0.99}Sr_{0.01}PO_{4-\delta}$ at $pO_2 = 0.01$ atm and $pH_2O = 0.041$ atm.

Table 1
Activation energies (eV) of electrical conductivity for the $Ce_{1-x}Sr_xPO_{4-\delta}$ series in selected conditions of atmosphere and temperature

$Ce_{1-x}Sr_xPO_{4-\delta}$ x	Conditions			
	Dry O_2 400–750 °C	Wet O_2 450–650 °C	Wet H_2 550–650 °C	Wet H_2 650–750 °C
0; bulk	0.57	0.53	–	–
0; total	0.56	0.49	–	–
0.01; bulk	–	0.43	0.85	0.77
0.01; total	0.46	–	0.86	0.80
0.02; bulk	–	0.44	0.78	0.59
0.02; total	0.44	–	0.76	0.58

Table 1. Neither Sr-doped nor undoped $CePO_4$ exhibited significant grain-boundary or electrode responses (Fig. 3). In the case of undoped $CePO_4$, the delineable bulk conductivity (Fig. 4) and corresponding activation energies are similar to the corresponding values for the total conductivity. For each composition, conductivities are comparable in wet and dry O_2; however, slightly higher values are observed in wet conditions at lower temperature, most noticeably for $x = 0$ and 0.01, in accordance with the data of Kitamura et al. [7] collected in wetter conditions.

The data conform to the expectation of higher concentrations of transport species with increasing acceptor-dopant concentration: the highest conductivity observed in the $Ce_{1-x}Sr_xPO_{4-\delta}$ system is exhibited by $x = 0.02$ in wet O_2. The conductivity increases from 3.38×10^{-5} S cm^{-1} at 600 °C for the undoped composition to 3.48×10^{-3} S cm^{-1} for $x = 0.02$. This increase in conductivity on doping $CePO_4$ is of the same order of magnitude as reported previously for 1 mol% Sr-doped material [7]. The absolute conductivity values of our study and the previous work (shown as solid lines in Fig. 4) are not directly comparable due to the different pO_2 levels taken for the Arrhenius plots in the two studies. Notwithstanding, on considering the observed trends of higher conductivity with increasing pO_2 and increasing dopant concentration, we may expect higher conductivities in the present study than the observed data. The discrepancies between the two studies may result from differences in both the synthesis conditions and morphologies of the samples. For example, at such small dopant concentrations, slight deviations in the stoichiometry or effects of porosity in our material are likely to moderate the conductivity. Nonetheless, the value for the E_a of the Sr-doped phase of 0.44 eV in oxidising conditions is equivalent (to within experimental error) to that reported previously (0.43 eV). The E_a of undoped $CePO_4$ in oxidising conditions, 0.56 eV, is slightly higher than the doped material, suggesting that the introduction of extrinsic defects alters the conduction mechanism in comparison to the undoped phase. It is likely that, in the latter, intrinsic defects arising from minor impurities and slight deviations from the ideal stoichiometry are of greatest influence on the transport behaviour.

The pO_2 dependence of total conductivity of composition $x = 0.02$ in the range $10^{-2.5} < pO_2 < 10^{-0.5}$ is shown in Fig. 5. The conductivity is approximately proportional to $pO_2^{+1/10}$ throughout the measured range below 800 °C, but at 800 °C a lower pO_2 dependence is observed.

For the discussion of defect chemistry, we adopt the approach of Kitamura et al. [7] in assuming that the defect behaviour of $CePO_4$ is similar to that of the better studied $LaPO_4$ proton-conducting system [8,9]. In this case, substitution of Ce with lower valence Sr results in the formation of oxygen vacancies, present as pyrophosphate ions at adjacent orthophosphate ion sites [7,8]:

$$\tfrac{1}{2}Sr_2P_2O_7 \rightarrow Sr'_{Ce} + \tfrac{1}{2}(P_2O_7)^{\bullet\bullet}_{2PO_4} \quad (5)$$

The oxygen vacancies may be charge compensated by electron holes on oxidation, localized on Ce as Ce^{4+} ions [7,8]:

$$(P_2O_7)^{\bullet\bullet}_{2PO_4} + \tfrac{1}{2}O_2 + 2Ce^x_{Ce} \Leftrightarrow 2Ce^{\bullet}_{Ce} + 2(PO_4)^x_{PO_4} \quad (6)$$

The equilibrium constant of oxidation (Eq.(5)) is

$$K_{Ox} = \frac{[Ce^{\bullet}_{Ce}]^2[(PO_4)^x_{PO4}]^2}{[(P_2O_7)^{\bullet\bullet}_{2PO4}][Ce^x_{Ce}]^2(pO_2)^{1/2}} \quad (7)$$

In a wet atmosphere, hydration of the pyrophosphate ions may also take place to form mobile protonic defects, $(HPO_4)^{\bullet}_{PO_4}$:

$$(P_2O_7)^{\bullet\bullet}_{2PO_4} + H_2O \Leftrightarrow 2(HPO_4)^{\bullet}_{PO_4} \quad (8)$$

The equilibrium constant of hydration (Eq. (8)) is

$$K_{Hydration} = \frac{[(HPO_4)^{\bullet}_{PO4}]^2}{[(P_2O_7)^{\bullet\bullet}_{2PO4}](pH_2O)} \quad (9)$$

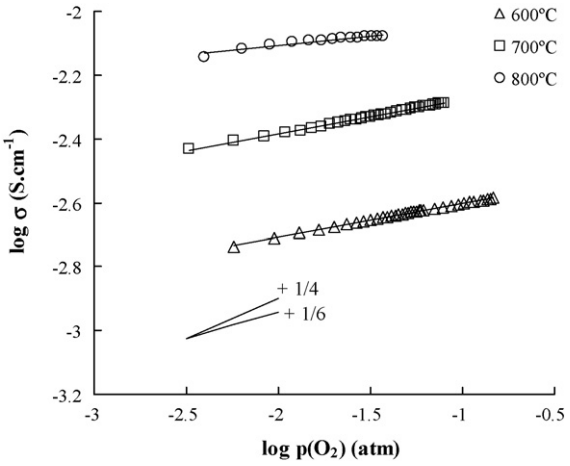

Fig. 5. Oxygen partial pressure dependence of the total conductivity of $Ce_{0.98}Sr_{0.02}PO_{4-\delta}$ in oxidising conditions.

At high humidities, hydration will be favoured, whereas at high oxygen partial pressures oxidation will be favoured. One can equate Eqs. (7) and (9) to give

$$\frac{K_{Ox}}{K_{Hydration}} = \frac{(pH_2O)[Ce_{Ce}^{\bullet}]^2[(PO_4)_{PO4}^{x}]^2}{[(HPO_4)_{PO4}^{\bullet}]^2[Ce_{Ce}^{x}]^2 pO_2^{1/2}} \quad (10)$$

The electroneutrality condition is

$$[(HPO_4)_{PO_4}^{\bullet}] + 2[(P_2O_7)_{2PO_4}^{\bullet\bullet}] + [Ce_{Ce}^{\bullet}] = [Sr_{Ce}'] + n \quad (11)$$

When all vacancies are filled (either by hydration or by oxidation), and assuming that under these conditions n-type conductivity is negligible, Eq.(11) can be simplified as

$$[(HPO_4)_{PO_4}^{\bullet}] + [Ce_{Ce}^{\bullet}] = [Sr_{Ce}'] \quad (12)$$

One also notes that both $[(PO_4)_{PO_4}^{x}] \gg [(P_2O_7)_{2PO_4}^{\bullet\bullet}]$ and $[Ce_{Ce}^{x}] \gg [Ce_{Ce}^{\bullet}]$ as the amount of Sr doping (and hence the concentration of Ce^{4+}) in these compositions is small. One can therefore state that $[(PO_4)_{PO_4}^{x}]$ and $[Ce_{Ce}^{x}]$ are almost constant. Under these conditions and at approximately constant pH_2O, Eqs.(10) and (12) can be combined to give

$$\frac{[Ce_{Ce}^{\bullet}]^2}{([Sr_{Ce}'] - [Ce_{Ce}^{\bullet}])^2} pO_2^{1/2} \quad (13)$$

Hence, p-type conductivity would be expected to exhibit a power-law dependence of $pO_2^{+1/4}$ when $[Sr_{Ce}'] \gg [Ce_{Ce}^{\bullet}]$, but this dependence would decrease with increasing Ce^{4+} concentration. In the situation that Sr is completely charge compensated by Ce^{4+}, no vacancies would be present, the p-type conductivity will tend to a constant and no hydration would be possible.

Moreover, one can note that rearrangement of Eq.(12) and substitution of $Ce_{Ce}^{\bullet}]$ with $[(HPO_4)_{PO_4}^{\bullet}]$ in Eq.(10) would give

$$\frac{[(HPO_4)_{PO_4}^{\bullet}]^2}{([Sr_{Ce}'] - [(HPO_4)_{PO_4}^{\bullet}])^2} pO_2^{1/2} \quad (14)$$

Thus proton conductivity would be expected to exhibit a dependence of $pO_2^{-1/4}$ when $[Sr_{Ce}\prime] \gg [(HPO_4)_{PO_4}{}^{\bullet}]$, i.e. when the formation of Ce^{4+} is the predominant charge-compensation mechanism; this negative dependence would decrease with increasing levels of hydration.

The conductivity behaviour shown in Fig. 5, shows a positive pO_2 power-law dependence of +1/10. From the previous discussion one could, therefore, suggest the dominance of p-type charge carriers, while evidence of mixed p-type and proton transport is provided by the slightly higher conductivity observed in wet with respect to dry oxidising regimes with similar partial-pressure dependencies. We assume in this argument that, in our studied temperature range, protons are the principal mobile ionic species and that oxygen-vacancy transport is relatively minor, as is the case in the isostructural La(Sr)$PO_{4-\delta}$ family [9]. Further work to systematically explore the role of water vapour and oxygen partial pressure on the transport properties in the acceptor-doped $CePO_4$ system is warranted.

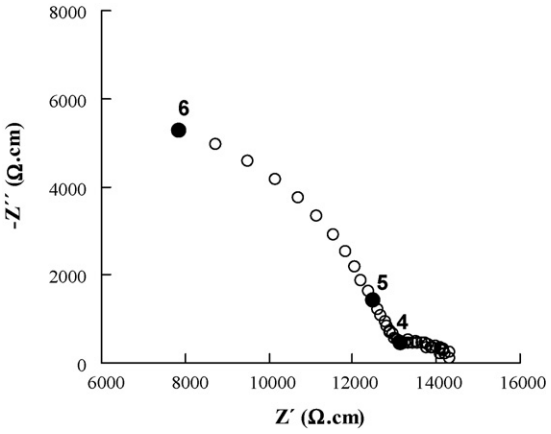

Fig. 6. Impedance spectrum of $Ce_{0.98}Sr_{0.02}PO_{4-\delta}$ in wet H_2 at 700 °C. Numbers refer to $\log_{10}$ of the frequency.

The resistance of $CePO_4$ in a reducing atmosphere of 10%H_2:90%N_2 was too large to be accurately measurable by the impedance analyser. Only an approximate estimate of the bulk conductivity was made for temperatures of 700 °C and above. The much higher conductivities of the Sr-doped phases, over two orders of magnitude greater than $CePO_4$, were determined over a wider range of temperatures. A typical impedance spectrum of $Ce_{0.98}Sr_{0.02}PO_{4-\delta}$ at 700 °C in wet H_2 is shown in Fig. 6. The capacitance of the major element was estimated (Eq. (4)) and again identified as that of the bulk (~18 pF). The second, lower-frequency contribution with a capacitance of $\sim 1.6 \times 10^{-7}$ F is most likely attributable to grain-boundary phenomena; this response was more apparent in reducing conditions in comparison to oxidising atmospheres.

Arrhenius plots of the bulk and total conductivities for samples measured in wet H_2 are shown in Fig. 7; corresponding activation energies are listed in Table 1; the lower conductivity estimated in dry conditions for the Sr-substituted phases is also shown. The activation energy of $Ce_{0.98}Sr_{0.02}PO_{4-\delta}$ in wet conditions in the temperature range 500–650 °C is 0.76 eV. There is a change to a lower activation energy regime around ~650 °C, which is consistent with the previously reported data

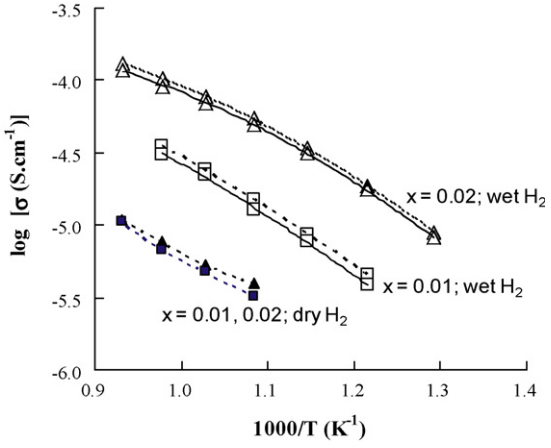

Fig. 7. Temperature dependence of the bulk (dashed line) and total (solid line) conductivity of the $Ce_{1-x}Sr_xPO_{4-\delta}$ series in wet and dry H_2.

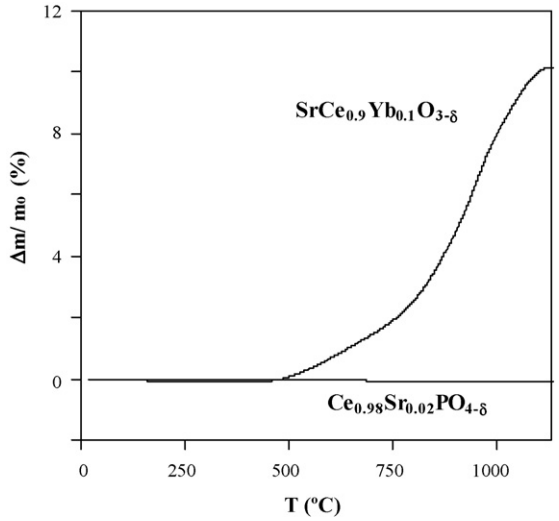

Fig. 8. Thermogravimetry of $Ce_{0.98}Sr_{0.02}PO_{4-\delta}$ and $SrCe_{0.9}Yb_{0.1}O_{3-\delta}$ in flowing CO_2.

[7] collected with higher pH_2O, ~0.4 atm. The slightly convex plot is likely to result from the loss of protonic charge carriers on dehydration at high temperature.

Although the $Ce(Sr)PO_{4-\delta}$ system apparently shows mixed protonic–electronic conduction, the conductivity is rather low for application in electrochemical devices, even in a thin-film configuration, very likely due to the low solubility of Sr in the $CePO_4$ parent phase.

3.3. Stability in CO_2

The monazite family of minerals is rather stable, whereas the Ba- and Sr-containing perovskite proton conductors suffer from poor stability in CO_2 due to carbonate formation, which limits the applicability of the perovskites as separator materials in electrochemical cells [4,18]. The stability of Sr-doped $CePO_4$ in a CO_2 atmosphere was assessed by TGA and compared to that of the well-known, proton-conducting perovskite material, $SrCe_{0.9}Yb_{0.1}O_{3-\delta}$ (Fig. 8). The monazite phase shows almost no weight change on heating in a CO_2 atmosphere, whereas the perovskite exhibits a large weight increase, as a result of reaction with CO_2 and decomposition to $SrCO_3$ and the remaining constituent oxides [4,18].

4. Conclusions

A solid-solution of $Ce_{1-x}Sr_xPO_{4-\delta}$ ($0 \leq x \leq 0.02$) with the monazite structure has been synthesized employing a nitrate-decomposition reaction, and evaluated in terms of electrical conductivity and stability in CO_2. Impedance spectra collected in wet and dry atmospheres of H_2 and O_2 are dominated by the bulk response. Conductivity increases with increasing dopant concentration, pO_2 and pH_2O. The transport behaviour is consistent with previously reported mixed protonic–electronic conduction. Analysis of data in the pO_2 range, $10^{-2.5}$ to $10^{-0.5}$ atm, indicates that hopping of electron holes (Ce^{4+}) is the dominant contribution to electronic transport. The rather low solubility limit of Sr ($x \sim 0.02$) limits the conductivity to values which are not yet suitable for potential electrochemical applications such as hydrogen-separation membranes. Nevertheless, the high stability in CO_2 and low cost of the alkaline-earth doped $CePO_4$ system indicates that $CePO_4$ is a promising host material for adopting other doping strategies which may achieve this end.

Acknowledgements

We would like to thank Delia Almudena Rey del Dedo (CSIC) and Alexei Yaremchecko (Universidade de Aveiro, Portugal) for technical assistance.

References

[1] S. Adhikari, S. Fernando, Hydrogen membrane separation techniques, Industrial & Engineering Chemistry Research 45 (2006) 875–881.
[2] T. Norby, Y. Larring, Mixed hydrogen ion–electronic conductors for hydrogen permeable membranes, Solid State Ionics 136–137 (2000) 139–148.
[3] J. Guan, S.E. Dorris, U. Balachandran, M. Liu, Transport properties of $BaCe_{0.95}Y_{0.05}O_{3-\alpha}$ mixed conductors for hydrogen separation, Solid State Ionics 100 (1997) 45–52.
[4] M.J. Scholten, J. Schoonman, J.C. van Miltenburg, H.A.J. Oonk, Synthesis of strontium and barium cerate and their reaction with carbon dioxide, Solid State Ionics 61 (1993) 83–91.
[5] S.-J. Song, T.H. Lee, E.D. Wachsman, L. Chen, S.E. Dorris, U. Balachandran, Defect structure and transport properties of Ni-$SrCeO_{3-\delta}$ cermet for hydrogen separation membrane, Journal of the Electrochemical Society 152 (2005) J125–J129.
[6] H. Matsumoto, T. Shimura, T. Higuchi, H. Tanaka, K. Katahira, T. Otake, T. Kudo, K. Yashiro, A. Kaimai, T. Kawada, J. Mizusaki, Protonic–electronic mixed conduction and hydrogen permeation in $BaCe_{0.9-x}Y_{0.1}Ru_xO_{3-\delta}$, Journal of the Electrochemical Society 152 (2005) A488–A492.
[7] N. Kitamura, K. Amezawa, Y. Tomii, T. Hanada, N. Yamamoto, T. Omata, S. Otsuka-Yao-Matsuo, Electrical conduction properties of Sr-doped $LaPO_4$ and $CePO_4$ under oxidizing and reducing conditions, Journal of the Electrochemical Society 152 (2005) A658–A663.
[8] T. Norby, N. Christiansen, Proton conduction in Ca- and Sr-substituted $LaPO_4$, Solid State Ionics 77 (1995) 240–243.
[9] S. Gallini, M. Hänsel, T. Norby, M.T. Colomer, J.R. Jurado, Impedance spectroscopy and proton transport number measurements on Sr-substituted $LaPO_4$ prepared by combustion synthesis, Solid State Ionics 162–163 (2003) 167–173.
[10] J.C.C. Abrantes, Sweep Control, Software Package, ESTG/IPVC, 2003.
[11] L. Haar, J.S. Gallagher, G.S. Kell, NBS/NRC Steam Tables, Hemisphere Publishing Corp, New York, 1984.
[12] J.C.C. Abrantes, J.R. Frade, ISA—Impedance Spectroscopy Analysis, Software Package ESTG/IPVC, 2003.
[13] B.A. Boukamp, A nonlinear least squares fit procedure for analysis of immittance data of electrochemical systems, Solid State Ionics 20 (1986) 31–44.
[14] M.J. Rampling, G.C. Mather, F.M.B. Marques, D.C. Sinclair, Electrical conductivity of hexagonal $Ba(Ti_{0.94}Ga_{0.06})O_{2.97}$ ceramics, Journal of the European Ceramic Society 23 (2003) 1911–1917.
[15] D. Poulidi, G.C. Mather, I.S. Metcalfe, Wireless electrochemical modification of catalytic activity on a mixed protonic–electronic conductor, Solid State Ionics 178 (2007) 675–680.
[16] G.C. Mather, F.M. Figueiredo, J.R. Jurado, J.R. Frade, Electrochemical behaviour of Ni-cermet anodes containing a proton-conducting ceramic phase on YSZ substrate, Electrochimica Acta 49 (2004) 2601–2612.
[17] E. Chinarro, J.R. Jurado, F.M. Figueiredo, J.R. Frade, Bulk and grain boundary conductivity of $Ca_{0.97}Ti_{1-x}Fe_xO_{3-\delta}$ materials, Solid State Ionics 160 (2003) 161–168.
[18] K.D. Kreuer, On the development of proton conducting materials for technological applications, Solid State Ionics 97 (1997) 1–15.